

2-9

各種鈍頭物体周りにおける高エンタルピー流れの数値計算

長友 英夫[†]、鹿野 信太郎[†]、山本 悟[‡]、大宮司 久明[‡][†] 東北大学大学院、[‡] 東北大学Numerical Simulation of Reactive and Non-reactive Hypersonic Flow Problems
for High Enthalpy Flow WorkshopHideo Nagatomo*, Shintaro Kano*,
Satoru Yamamoto** and Hisaaki Daiguji**

* Graduate School of Tohoku University

** Tohoku University

Abstract

Numerical simulations of hypersonic flow assuming no reaction and thermochemical nonequilibrium are performed. Three different methods, Implicit-Explicit Flux Vector Splitting(IEFVS), AUSM and AUSM_DV scheme are used. All of these schemes are coupled with Fourth-order MUSCL TVD scheme in space which enable us to capture vortices more clearly. AUSM scheme is applied for non-reactive flow problems, the flow around OREX (Test case problem II-5), and hyperboloid flare (III-1). On the other hand, for the thermochemical nonequilibrium flow problems, such as the flow around OREX (II-2) are calculated by the IEFVS and AUSM_DV scheme. The spherically blunted cone (IV-1) is done by the IEFVS.

1. Introduction

For the numerical simulation of hypersonic viscous flows, the computational method should be very robust for shocks and numerically non-dissipative in the boundary layer. To satisfy them, some methods have been already proposed. The authors also have developed a method based on Implicit-Explicit Flux Vector Splitting (IEFVS) for the simulation of thermochemical nonequilibrium hypersonic viscous flow[1]. This scheme is very robust for obtaining the bow shock because of the characteristic of the FVS scheme, accurate in the boundary layer by using the Roe's averaging and quite simple for the almost same formation of both implicit and explicit terms. We also know robust schemes, AUSM and AUSM_DV scheme, therefore, these schemes are also used to check reliability for the present flow problems.

On the other hand, fourth-order compact MUSCL TVD[2] is used to obtain higher-resolution results, with each IEFVS, AUSM, AUSM_DV scheme.

In this paper, the numerical procedure of discretization is firstly explained briefly and flow problems given as the present workshop subject, the flow around OREX (II-2, II-5), the hyperboloid flare (III-1) and the spherically blunted cone (IV-1) are considered. The problem II-5 and III-1 are calculated by the AUSM, the problems II-2 is calculated by the IEFVS and the AUSM_DV, and the problems IV-1 is calculated by the IEFVS.

2. Numerical Method

2.1 Fundamental Equations The two-dimensional conservation equations for the thermochemical nonequilibrium flow are expressed as follows.

$$\frac{\partial Q}{\partial t} + \frac{\partial F_i}{\partial \xi_i} + S + H = 0 \quad (1)$$

Q is the vector of unknown variables, $Q = J(\rho_s, \rho u_1, \rho u_2, E, E_v)$, where ρ is the total density and ρ_s is each density of species s . F_i , S and H are the flux, the diffusion term and the source term respectively, and they are described as follows.

$$F_i = J \begin{bmatrix} \rho_s U_i \\ \rho u_1 U_i + \partial \xi_i / \partial x_1 p \\ \rho u_2 U_i + \partial \xi_i / \partial x_2 p \\ (E + p) U_i \\ E_v U_i \end{bmatrix}$$

$$S = -J \frac{\partial \xi_i}{\partial x_j} \frac{\partial}{\partial \xi_i} \begin{bmatrix} -\rho_s v_{sj} \\ \tau_{1j} \\ \tau_{2j} \\ \tau_{1j} u_i - q_j - \sum_{s \neq e}^n \rho_s v_{sj} h_s \\ -q_{vj} - \sum_{s \neq e}^m \rho_s c_{vs} v_{sj} \end{bmatrix}$$

$$H = -J \begin{bmatrix} w_s \\ 0 \\ 0 \\ 0 \\ W_v \end{bmatrix}, \quad (s = 1, \dots, n, i = 1, 2)$$

For reacting flow, 7 chemical species (N_2 , O_2 , NO , NO^+ , N , O , e^-) are considered so that the system includes 11 equations here. Models for chemical reactions and the vibrational relaxation time in the source term H are quoted from Park[5] and Candler[6] mainly. The total energy E , the pressure p , and the gas constant are given below.

$$E = \sum_{s \neq e} \rho_s C_{v,s} T + \frac{1}{2} \rho u_j u_j + E_v$$

$$+ \sum_{s \neq e} \rho_s h_s^0 + \sum_{s \neq e} \rho_s e_{els}$$

$$p = \sum_{s \neq e} \rho_s \frac{R}{M_s} T + p_e, \quad \bar{R} = \sum_{s \neq e} \frac{\rho_s R}{\rho M_s}$$

$C_{v,s}$, T , h_s^0 , e_{els} , R , M_s , p_e means the translational specific heat, translational-rotational temperature, heat of formation of species s , universal gas constant, atomic weight of species s and the electron pressure respectively.

2.2 Discretization

The numerical flux of F_i in eq.(1) are defined as the linearized flux vector forms.

$$(F_i)_{t+1/2}^n = (A_i^+)_{t+1/2} Q_{t+1/2}^L + (A_i^-)_{t+1/2} Q_{t+1/2}^R \quad (2)$$

The superscripts L and R in the vector of unknown variables, $Q_{t+1/2}^L$ and $Q_{t+1/2}^R$ mean the weighted extrapolation from the right and left by the MUSCL approach, and they are calculated by the following equations.

$$Q_{t+1/2}^L = Q_t + \frac{1}{6} \Delta^+ \bar{Q}_{t-1/2} + \frac{1}{3} \Delta^- \bar{Q}_{t+1/2}$$

$$Q_{t+1/2}^R = Q_{t+1} - \frac{1}{6} \Delta^- \bar{Q}_{t+3/2} - \frac{1}{3} \Delta^+ \bar{Q}_{t+1/2} \quad (3)$$

where $\Delta^\pm \bar{Q}$ are the numerical functions composed of ordinary third-order term and fourth-order compact term.

On the other hand, if the LU-SGS scheme by Yoon et.al.[7] and point-implicit method by Eberhardt[8] are used, eq.(1) can be written in the implicit form as

$$[I + \Delta t \{ \beta \sigma(A_i) + \text{diag}(\frac{1}{\tau}) + \text{diag}(\alpha_j) \}] \delta Q = RHS$$

$$- \Delta t \{ (A_j^-)_{t+1/2} \delta Q_{t+1} - (A_j^+)_{t-1/2} \delta Q_{t-1} \} \quad (4)$$

where

$$RHS = -\Delta t (\Delta F_i^n + S^n + H^n)$$

In eq.(4), $\sigma(A_i)$ is an identity matrix with the spectral radius of A_i . In this paper, the maximum of absolute eigenvalues for A_i is taken. $1/\tau \equiv 1/\tau_s$ (

$s = 1, \dots, n$ and E_v) is quoted from Ref.[8] and α_j is set to $2\mu g_{jj}/(Re\rho\Delta\xi_j)$.

Next, the Implicit-Explicit Flux Vector Splitting (IEFVS) is explained. The distinctive feature is that it is applicable to both explicit and implicit calculations. It means that not only the flux $A_i^\pm Q$, but the flux $A_i^\pm \delta Q$ can be calculated from a same flux-vector splitting form. This form can be written in the vector form composed of sub-vectors as

$$A_i^\pm \bar{Q} = J \begin{bmatrix} \bar{q}_s \\ \bar{q}_{u_1} \\ \bar{q}_{u_2} \\ \bar{q}_e \\ \bar{q}_{e_v} \end{bmatrix} \lambda_{i1}^\pm$$

$$+ \frac{J}{c\sqrt{g_{ii}}} \begin{bmatrix} 0 & + & \bar{q}_s/\bar{q}_0 \cdot \Delta \bar{U}_i \\ \xi_{i,1}\bar{p} & + & \bar{q}_{u_1}/\bar{q}_0 \cdot \Delta \bar{U}_i \\ \xi_{i,2}\bar{p} & + & \bar{q}_{u_2}/\bar{q}_0 \cdot \Delta \bar{U}_i \\ \bar{U}_i\bar{p} & + & (\bar{\chi}^2 + c^2)/\bar{\gamma} \cdot \Delta \bar{U}_i \\ 0 & + & \bar{q}_{e_v}/\bar{q}_0 \cdot \Delta \bar{U}_i \end{bmatrix} \lambda_{ia}^\pm$$

$$+ \frac{J}{c^2} \begin{bmatrix} \bar{q}_s/\bar{q}_0 \cdot \bar{p} & + & 0 \\ \bar{q}_{u_1}/\bar{q}_0 \cdot \bar{p} & + & \xi_{i,1}c^2/g_{ii} \cdot \Delta \bar{U}_i \\ \bar{q}_{u_2}/\bar{q}_0 \cdot \bar{p} & + & \xi_{i,2}c^2/g_{ii} \cdot \Delta \bar{U}_i \\ (\bar{\chi}^2 + c^2)/\bar{\gamma} \cdot \bar{p} & + & \bar{U}_i c^2/g_{ii} \cdot \Delta \bar{U}_i \\ \bar{q}_{e_v}/\bar{q}_0 \cdot \bar{p} & + & 0 \end{bmatrix} \lambda_{ib}^\pm \quad (5)$$

where

$$\bar{p} = \bar{q}_0 \bar{\phi}^2 - \bar{\gamma}(\bar{q}_{u_1}\bar{q}_{u_1} - \bar{q}_0\bar{q}_e - \bar{q}_0\bar{q}_{e_v})/\bar{q}_0$$

$$\bar{\phi}^2 = \bar{\gamma}(\bar{q}_{u_1}\bar{q}_{u_1}/2\bar{q}_0^2$$

$$- \sum_{s \neq e} \bar{q}_s h_s^0/\bar{q}_0 - \sum_{s \neq e} \bar{q}_s e_{els}/\bar{q}_0)$$

$$\bar{\chi}^2 = \bar{\gamma}(\bar{q}_{u_1}\bar{q}_{u_1}/2\bar{q}_0^2 + \bar{q}_{e_v}/\bar{q}_0$$

$$+ \sum_{s \neq e} \bar{q}_s h_s^0/\bar{q}_0 + \sum_{s \neq e} \bar{q}_s e_{els}/\bar{q}_0)$$

$$\Delta \bar{U}_i = \xi_{i,j}\bar{q}_{u_j} - \bar{q}_0\xi_{i,j}\bar{q}_{u_j}/\bar{q}_0$$

$$\lambda_{ij}^\pm = (\lambda_{ij} \pm |\lambda_{ij}|)/2 \quad (j = 1, 3, 4)$$

$$\lambda_{ia}^\pm = (\lambda_{i3}^\pm - \lambda_{i4}^\pm)/2$$

$$\lambda_{ib}^\pm = (\lambda_{i3}^\pm + \lambda_{i4}^\pm)/2 - \lambda_{i1}^\pm$$

If we use eq.(5) in the explicit calculation, then $\bar{Q} = (\bar{q}_s, \bar{q}_{u_1}, \bar{q}_{u_2}, \bar{q}_e, \bar{q}_{e_v})$ is specified to Q . On the other hand, \bar{Q} is set to δQ if it is for the implicit calculation. We need no additional calculations such as matrices for eigenvectors. The values with upper bar are estimated by the Roe's averaging to overcome the excessive dissipation in the boundary layer.

AUSM scheme by Liou et.al.[3] and AUSM-DV scheme by Wada et.al.[4] are also applied here with fourth-order compact MUSCL TVD scheme.

3. Results

3.1 Non-reactive flows

Problem II-5. The axisymmetric non-reactive laminar flows around OREX is simulated. Outer boundary conditions are set to $u_{\infty} = 5562$ [m/sec], $p_{\infty} = 23.60$ [Pa], $T_{\infty} = 248.1$ [K] and the wall temperature is $T_{wall} = 1519$ [K].

The computational mesh has 95×95 grid points. (Fig.1) In this calculation, the AUSM scheme with the fourth-order compact MUSCL TVD is used to verify the capability of its application. Fig.2 to 5 show the temperature contours, pressure contours, pressure distribution and the heat flux distribution on the body surface. The shock distance from the nose is about 0.19m.

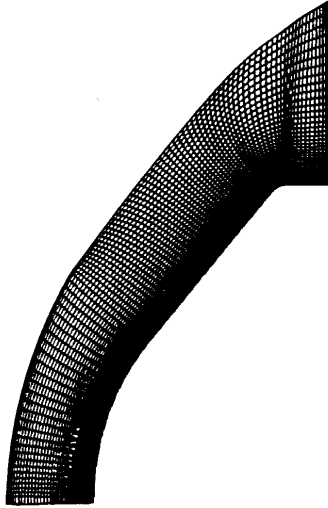


Fig.1 Computational mesh(95×95 grid points)

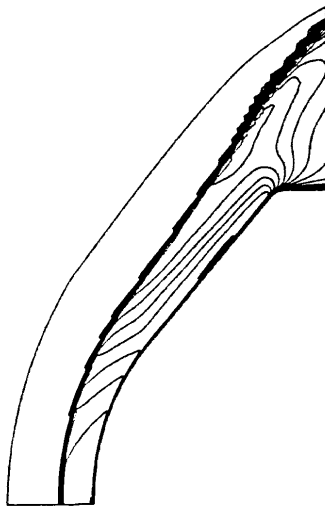


Fig.2 Temperature Contours

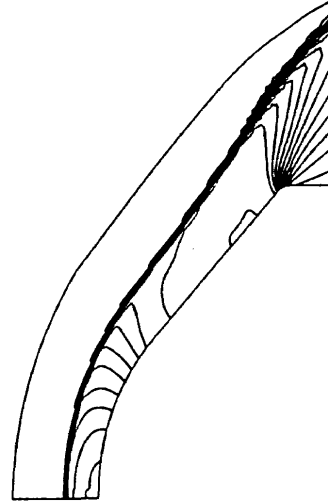


Fig.3 Pressure Contours

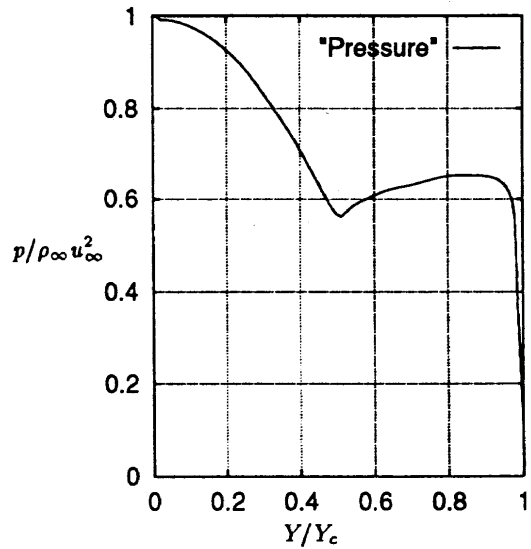


Fig.4 Pressure distribution on the surface

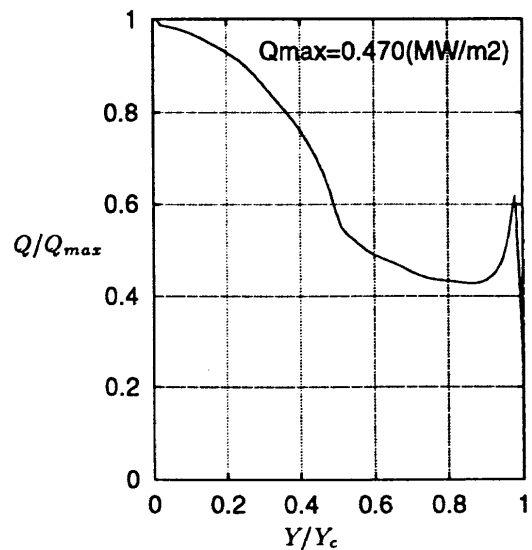


Fig.5 Heat flux distribution on the surface

Problem III. The axisymmetric non-reactive laminar flow around hyperboloid flare is simulated also by the same scheme of II-5. The computational mesh has 521×101 grid points which was provided by the workshop organizer.(Fig.6) The experimental data of the Geottingen Ludwig Tube (Cold Case) was used for the condition of this calculation. Outer boundary conditions are set to $M_\infty = 6.83$, $Re_\infty/m = 7.0 \times 10^6$, $T_\infty = 67.765$ [K] and the wall temperature is $T_{wall} = 310$ [K]. Calculations both by fourth-order and first-order accuracy in space were executed.

Figs.7 and 8 show the calculated results of pressure contours and temperature contours by first-order scheme respectively and Figs. 9 and 10 show the same results by fourth-order one.

In the latter results, a large separation area near the compression corner and shock interactions are captured clearly, though small oscillations are visible. The separation point of fourth-order case estimated from pressure distributions (Fig.11) is about $X_{separate}/X_{ref} = 0.62$. The reason of the oscillations is unconsiderable here, but this should be deleted.

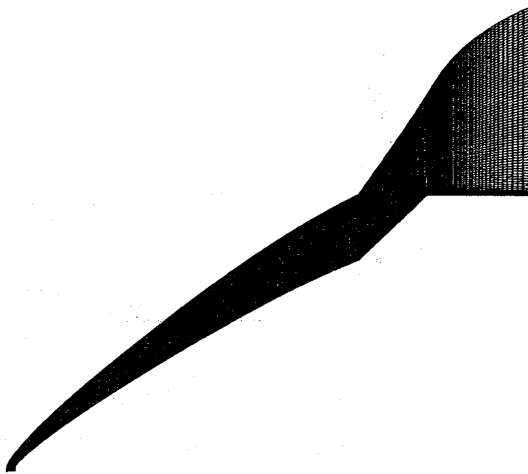


Fig.6 Computational mesh(521×101 grid points)

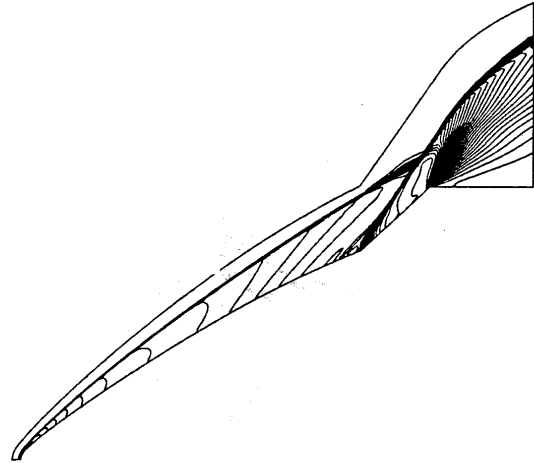


Fig.7 Pressure Contours (First-order)

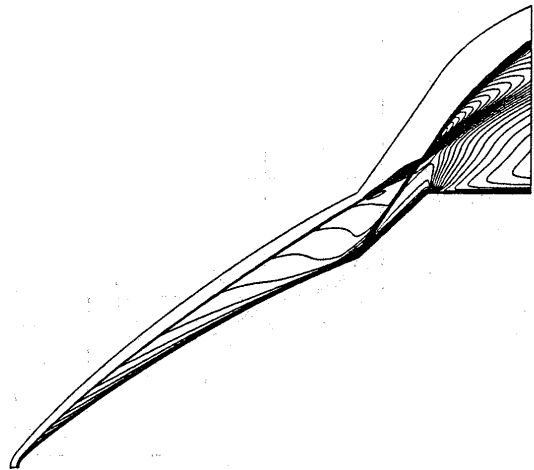


Fig.8 Temperature Contours (First-order)

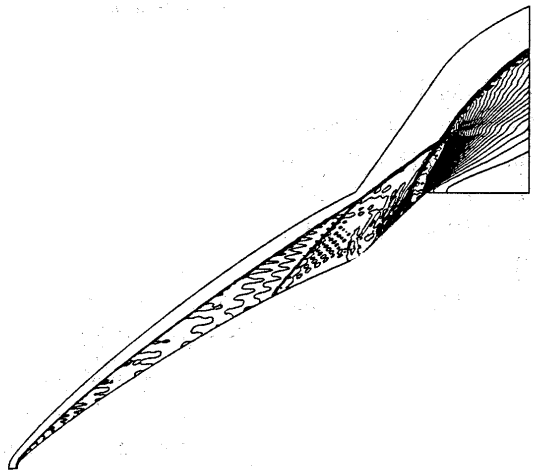


Fig.9 Pressure Contours (Fourth-order)

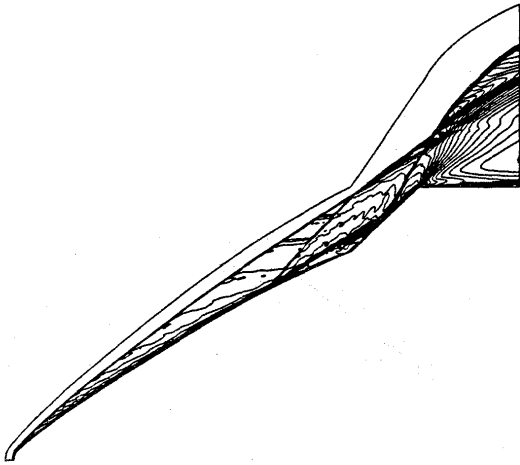


Fig.10 Temperature Contours (Fourth-order)

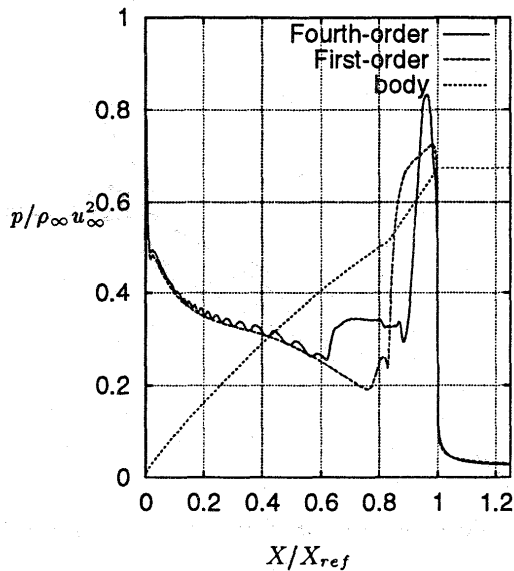


Fig.11 Pressure distributions

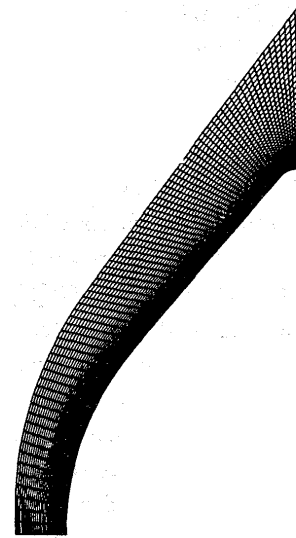


Fig.12 Computational mesh(75 x 75 grid points)

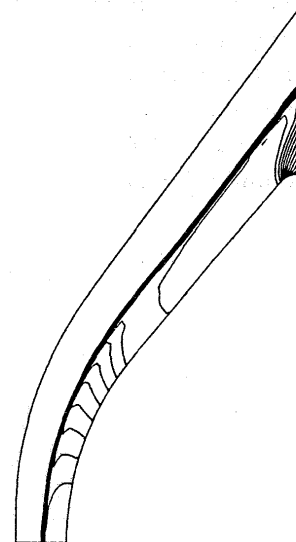


Fig.13 Pressure contours (IEFVS)

3.2 Reactive flows

Problem II-2. The computational mesh has 75×75 grid points.(Fig.12) Outer boundary conditions are set to $u_\infty = 5562$ [m/sec], $p_\infty = 23.60$ [Pa], $T_\infty = 248.1$ [K] and the wall temperature is $T_{wall} = 1519$ [K].

In this calculation, IEFVS and AUSM.DV schemes with fourth-order compact MUSCL TVD are used. Figs. 13 and 14 show the calculated results of pressure contours and translational-rotational temperature contours respectively by IEFVS scheme and Figs.15 and 16 show those results by AUSM.DV scheme. Fig.17 shows the temperature distributions on the stagnation streamlines. These results are similar and the shock distance from the nose by FVS is 10.9cm. On the other hand, that by AUSM.DV is slightly less than that of FVS. However the difference is only a length between a grid point and next one.

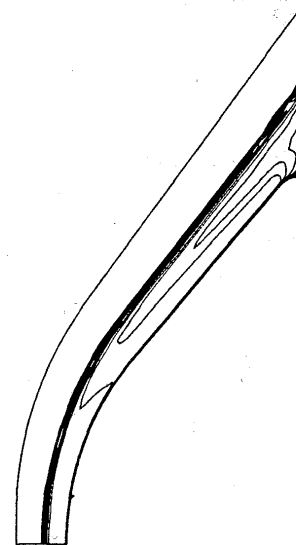


Fig.14 Translational-rotational temperature contours (IEFVS)

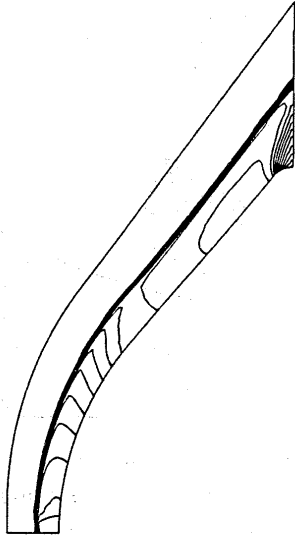


Fig.15 Pressure contours (AUSM_DV)

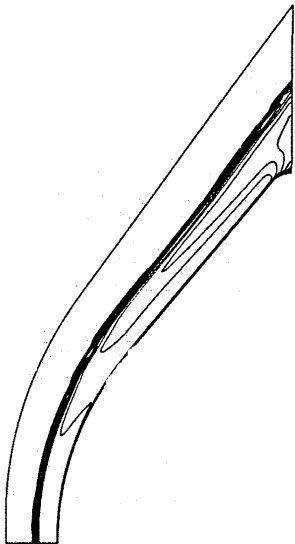


Fig.16 Translational-rotational temperature contours (AUSM_DV)

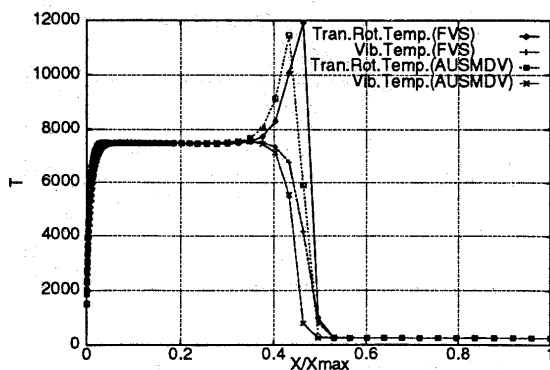


Fig.17 Temperature distributions on stagnation streamline

Problem IV-1. The axisymmetric laminar flow with chemical reacting around the spherically blunted cone is simulated. The computational mesh

used here is shown in Fig.18 which was provided by the workshop organizer. Outer boundary conditions are set to $u_{\infty} = 4539.5$ [m/sec], $p_{\infty} = 588.42$ [Pa], $T_{\infty} = 489.89$ [K] and the wall temperature is $T_{wall} = 295$ [K].

The calculation was performed by IEFVS with fourth-order and first-order accuracy in space. Figures 19 to 21 show the calculated results of pressure contours, translational-rotational temperature contours and vibrational temperature contours respectively by the fourth-order scheme and Figs. 22 to 24 show those results by the first-order. From the comparison of these figures, the further rear stagnation point from the base is obtained by the fourth-order case than by first-order. This reason may be due to the capability of capturing separation points and vortices. Figure 25 shows the heat flux distributions of the calculated results and that of experimental data[9], where S means the distance along the body surface from the front stagnation point. The fourth-order result has a peak at the almost same position as that of experimental one whereas the value at the point is smaller. However, it seems to be at least necessary to apply higher-order scheme to simulate base region in hypersonic flow.

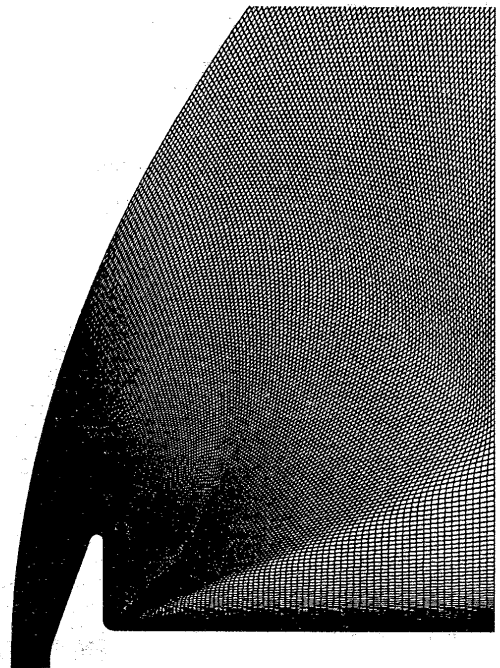


Fig.18 Computational mesh(161 × 241 grid points)

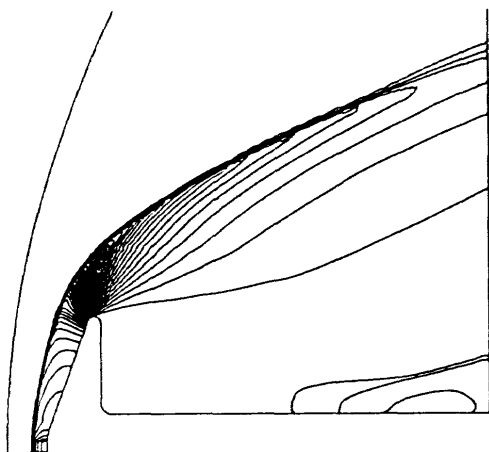


Fig.19 Pressure contours
(Fourth-order)

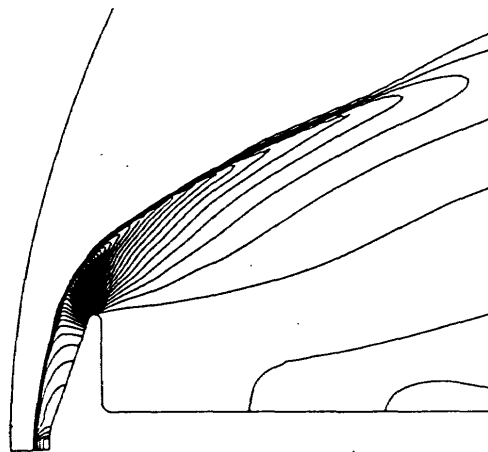


Fig.22 Pressure contours
(First-order)

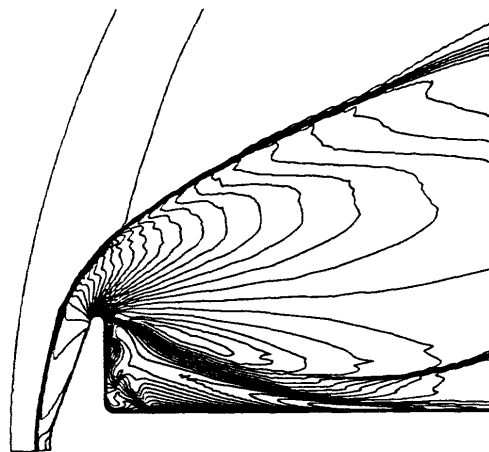


Fig.20 Translational-rotational temperature
contours (Fourth-order)

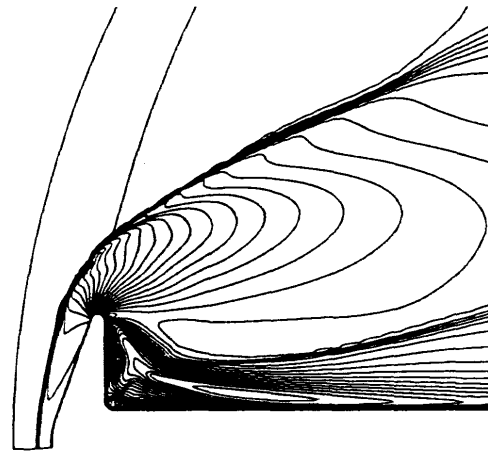


Fig.23 Translational-rotational temperature
contours (First-order)

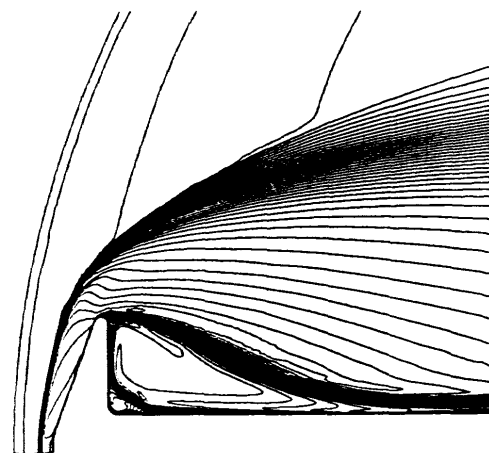


Fig.21 Vibrational temperature contours
(Fourth-order)

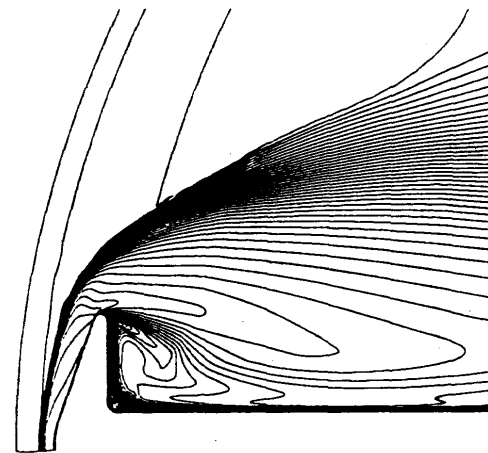


Fig.24 Vibrational temperature contours
(First-order)

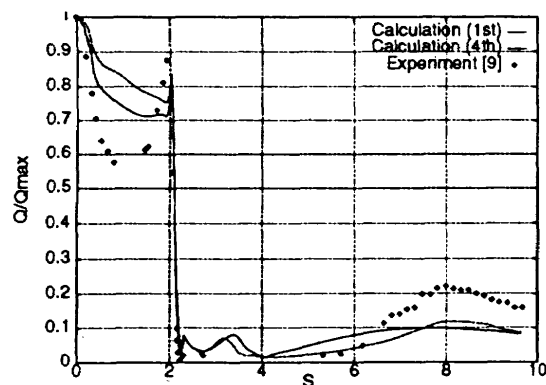


Fig.25 Heat flux distribution

4. Conclusion

Numerical simulations are performed for High Enthalpy Flow Workshop problems. The AUSM scheme was very effective for non-reactive problem. However, the oscillation in higher-order case of II-5 should be overcome in future. The AUSM-DV and IEFVS with the higher-order accuracy were equivalently effective for the reacting flow problem II-2. The last case IV-1 indicates the necessity of higher-order accuracy at the wake region after the body. By the way, the result by the AUSM-DV for the last case is not shown because of still having a problem in the result. It must be also resolved.

References

- [1] Yamamoto, S., Nagatomo, H. and Daiguji, H., *Proc. of the 14th International Conf. on Numerical Methods in Fluid Dynamics, Lecture Notes in Phys.*, Springer-Verlag (1995), pp.314-319.
- [2] Yamamoto, S. and Daiguji, H., *J. Comput. & Fluids*, Vol.22, No.2/3, (1993), pp.259-270.
- [3] Liou, M.-S. and Steffen, C.J., *J. Comput. Phys.*, Vol.107, (1993), pp.23-39.
- [4] Wada, Y. and Liou, M.-S., AIAA Paper 94-0083, (1994).
- [5] Park, C. and Yoon, S., *J. Spacecraft and Rockets*, Vol.1 (1991), pp.31-39.
- [6] Candler, G., Ph.D Thesis, Stanford University, (1988).
- [7] Imlay, S.T. and Eberhardt, S., AIAA Paper 91-0468, (1991).
- [8] Park, C. and Yoon, S., *J. Spacecraft and Rockets*, Vol.28, No.1, (1991), pp.31-39.
- [9] Kastell, D., Horvath T. J. and Eitelberg, G., *Proc. of the Second European Symp. on Aerothermodynamics for Space Vehicles*, (1994), pp.383-389.